Semantic-Aware and Quality-Aware Interaction Network for Blind Video Quality Assessment

Anonymous Author(s)

ABSTRACT

Current state-of-the-art video quality assessment (VQA) models typically integrate various perceptual features to comprehensively represent video quality degradation. These models either directly concatenate features or fuse different perceptual scores while ignoring the domain gaps between cross-aware features, thus failing to adequately learn the correlations and interactions between different perceptual features. To this end, we analyze the independent effects and information gaps of quality- and semantic-aware features on video quality. Based on an analysis of the spatial and temporal differences between two aware features, we propose a semantic-**A**ware and quality-**A**ware **I**nteraction **Net**work (**A^{2}INet**) for blind VQA. For spatial gaps, we introduce a cross-aware guided interaction module to enhance the interaction between semantic- and quality-aware features in a local-to-global manner. Considering temporal discrepancies, we design a cross-aware temporal modeling module to further perceive temporal content variation and quality saliency information, and perceptual features are regressed into quality score by a temporal network and a temporal pooling. Extensive experiments on six benchmark VQA datasets show that our model achieves state-of-the-art performance, and ablation studies further validate the effectiveness of each module. We also present a simple video sampling strategy to balance the effectiveness and efficiency of the model. The code for the proposed method will be released.

CCS CONCEPTS

• **Computing methodologies** → Modeling and simulation.

KEYWORDS

Video quality assessment, semantic- and quality-aware, cross-aware guided interaction, cross-aware temporal modeling.

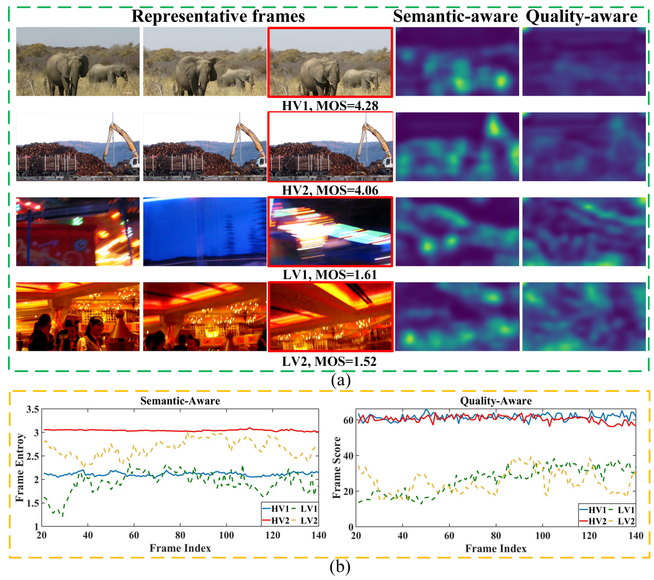

Figure 1: Visualize the spatial feature maps of semantic- and quality-aware, alongside the temporal distribution of features on two high-quality videos (HV1 and HV2) and two low-quality videos (LV1 and LV2). MOS is the mean opinion score, higher values mean better subjective visual quality. (a) Three representative frames, and the semantic- and quality-aware feature maps are presented for the frames boxed in red. We use ResNet-50 [13] pre-trained on the ImageNet dataset [7] and the KoNIQ-10k dataset [15] to generate the semantic- and quality-aware feature maps. (b) The temporal distribution of each aware feature. Frame entropy and frame score for each frame of the feature map are used to measure information content and image quality, respectively.

1 INTRODUCTION

The goal of video quality assessment (VQA) is to enable the model to perceive the visual quality of videos and produce results consistent with human subjective opinions, making it a popular research topic in multimedia [21, 45]. Blind VQA (BVQA) models evaluate video quality in the absence of reference videos, so huge efforts for BVQA have been devoted and a variety of deep learning-based models have been proposed [47, 59].

Given that human judgments of video quality are influenced by multiple perceptual factors working in concert, recent top models [47, 56] that adopt multiple networks to extract perceptual features, resulting in superior performance over models using a single network [23, 53]. These models concatenate features or fuse quality scores from different branches to comprehensively represent video quality. However, domain gaps between different aware features remain under-studied in existing work, hindering the full utilization of the advantages of multiple features in VQA and further constraining the perceptual ability of the models.

Subjective studies are instructive for the design of objective VQA models, and previous studies [43, 47] indicate that visual content and distortion artifacts play primary roles in human judgments of video quality. Visual content primarily pertains to content composition and motion information, which dominate human preferences for video content and are referred to as semantic-aware. Distortion

Permission to make digital or hard copies of all or part of this work for personal or classroom use is granted without fee provided that copies are not made or distributed for profit or commercial advantage and that copies bear this notice and the full citation on the first page. Copyrights for components of this work owned by others than ACM must be honored. Abstracting with credit is permitted. To copy otherwise, or republish, to post on servers or to redistribute to lists, requires prior specific permission and/or a fee. Request permissions from permissions@acm.org.
MM '24, October 28–November 1, 2024, Australia, Melbourne
© 2024 Association for Computing Machinery.
ACM ISBN 978-1-4503-XXXX-X/18/06…$15.00
https://doi.org/XXXXXXX.XXXXXXX

artifacts such as spatial degradation and temporal flicker are introduced into video due to imperfections in capture equipment or processing algorithms, which is denoted as quality-aware. Taking two sets of videos with varying quality levels, as depicted in Figure 1, as examples, we analyze the roles of semantic- and quality-aware features in VQA. **Two aware features focus on distinct spatial perceptual information by comparing videos with varying qualities from Figure 1(a).** The semantic-aware features focus on objects and are robust to quality degradation, while the quality-aware features are sensitive to quality degradation and exhibit a stronger response in low-quality frames. Thus, combining two aware features spatially can better understand the quality degradation in context. **Two aware features exhibit different temporal characteristics by observing Figure 1(b).** High-quality videos (**blue and red solid curves**) have slower fluctuations in temporal content information and higher frame-level quality. The opposite is true for low-quality videos (**green and yellow dashed curves**). Temporal content variations and overall quality emerge as key factors in discerning video quality degradation. In summary, cross-aware features exhibit perceptual gaps across spatial and temporal dimensions. We argue that simply concatenating features makes it difficult to comprehend the intricate connections between different perceptual features and video quality.

To address these challenges, we propose an effective and efficient semantic-**A**ware and quality-**A**ware **I**nteraction **Net**work (**A^{2}INet**) for BVQA. To mitigate representation differences and enhance spatial perception, we propose a cross-aware guided interaction (CAGI) module that uses cross-aware guided instance normalization (CGIN) to perceive the gaps between frame-level features with semantic- and quality-aware features, and then implements global interaction through a global self-attention layer. Motivated by Figure 1(b), we design a cross-aware temporal modeling (CATM) module by capturing information with significant quality degradation and content variation to enhance the perception for temporal distortion. Finally, the video quality score is obtained through temporal modeling and temporal pooling for the perceptual features. We conduct extensive experiments to verify that the proposed BVQA model achieves state-of-the-art (SOTA) results on the LIVE-Qual [11], CVD2014 [33], LIVE-VQC [37] and KoNViD-1k [14] datasets, with respective improvements of **7.25%, 2.43%, 4.92% and 3.95% in Spearman rank order correlation coefficient (SRCC)**. The main contributions of this paper are as follows,

1) As far as we know, this is the first attempt to explore differences in various perceptual features and employ cross-aware feature learning to enhance the perceptual ability of models for BVQA.

2) We design a CAGI module comprising a CGIN and a global self-attention layer, it uses a local-to-global manner to facilitate interaction on two aware features.

3) We introduce a CATM to perceive temporal distortions from the perspectives of quality saliency and content variation.

4) Extensive experiments have verified the advantages of the proposed BVQA model, and ablation studies have demonstrated the effectiveness of each module.

2 RELATED WORK

The success of the BVQA model hinges on effective perceptual feature extraction and temporal modeling to represent video quality degradation across spatial and temporal dimensions.

2.1 Feature extraction for BVQA

BVQA models based on hand-crafted features. Classic BVQA methods [6, 19, 25, 32, 35, 40] are designed to use hand-crafted features for describing visual quality degradation. Nevertheless, these hand-crafted features only emphasize low-level edges and texture information, falling short of capturing high-level semantic information. Subsequent work [20, 41] combined hand-crafted features with semantic features extracted from pre-trained ResNet-50 [13] models, yielding promising results.

BVQA models based on deep features. Deep learning-based models are further divided into **fixed backbone** [22, 58] and **end-to-end training** [44, 59] methods. Fixed backbone-based methods extract features from video using feature extractors pre-trained on other tasks. Li *et al.* [23, 24] used a pre-trained ResNet-50 to extract content-aware features. Related researches [3, 26] follow the work of [23, 24] using a single 2D network to capture features. Madhusudana *et al.*[31] proposed self-supervised learning to train the feature encoder. Many researches [22, 43, 51, 52, 58] have designed multiple backbone networks and concatenated features to capture various information from distorted videos, and obtained better results than a single network. Zhang *et al.* [56] incorporated five features related to visual perception and achieved SOTA performance.

For end-to-end training methods, early models [4, 53] utilized single convolutional neural networks (CNN) to extract perceptual features. Recently, Wu *et al.* [44, 45] proposed FAST-VQA, which takes video fragments as inputs and trains variants of the video swin Transformer tiny (SwinT-3D) [29] for BVQA. DisCoVQA [46] trained SwinT-3D with sparse frames as input. Yuan *et al.* [55] designed a video transformer with a multi-path temporal network and sparse attention blocks for capturing different distortions. Sun *et al.* [38] fine-tuned ResNet-50 and incorporated motion features to represent video quality. ZoomVQA [59] trained the image quality assessment (IQA) and VQA branches separately. Wu *et al.* [47] used inflated-ConvNext [28] and FAST-VQA models to perceive the quality of aesthetic and technical perspectives, obtaining video quality scores through simple weighted fusion.

Overall, existing models usually concatenate features or fuse branch scores to predict video quality. We analyze spatial gaps in different aware features to narrow the feature gaps and enhance mutual perception through a CAGI module. Since this paper focuses on exploring more effective ways of combining different aware features for BVQA rather than feature extraction, the proposed model is designed as a fixed backbone method.

2.2 Temporal modeling for BVQA

Temporal distortion primarily occurs in the form of flicker, jitter, and scene transitions, leading to video quality degradation. Previous studies have shown that temporal modeling is crucial for BVQA.

Li *et al.* [23, 24] modeled temporal relationships frame-by-frame using gated recurrent units (GRUs) [5], employing both min pooling and soft-weighted average pooling to aggregate frame-level

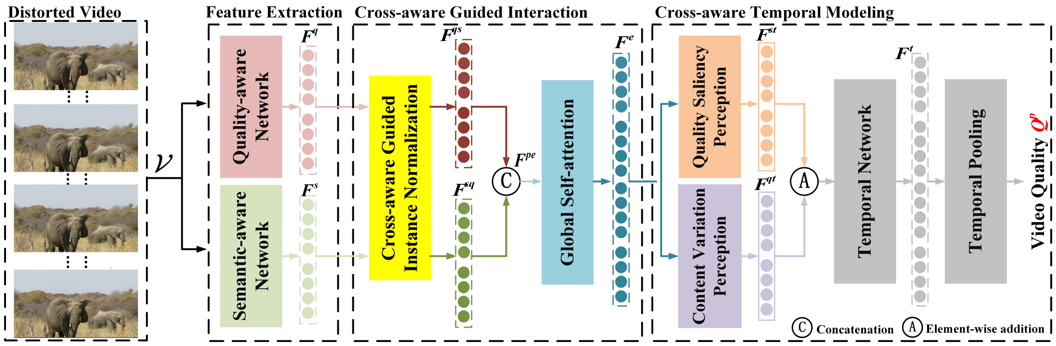

Figure 2: The framework of the proposed A^{2}INet for BVQA, with the feature extraction module (Section 3.1) to extract two aware features, the CAGI (Section 3.2) to perform local and global interactions of two aware features, and CATM module (Section 3.3) to capture the long-term dependencies of fused features and regress features into video quality scores.

scores. [22, 56] referenced this temporal modeling and temporal pooling method. Chen *et al.* [4] introduced multi-level GRUs to fuse motion information of different frequencies. Chen *et al.* [3] designed a pyramid temporal aggregation module that fuses short-term and long-term memory of frame-level features. Telili *et al.* [39] utilized bidirectional long short-term networks (Bi-LSTM) to capture temporal correlations between the previous and next frames. Ying *et al.* [52] used InceptionTime [17] for temporal modeling due to its faster and easier training. Li *et al.* [26] proposed a hierarchical Transformer that integrates frame-level and clip-level quality to derive video-level quality scores by stacking several divide and conquer Transformer layers. Wu *et al.* [46] designed a temporal content Transformer to learn the relationships among frame contents. In addition to modeling the long-term dependencies of video frames through temporal networks, some related works [22, 38, 44, 46–48, 58, 59] employed 3D networks, such as SlowFast [9], Swin-Transformer (Swin-3D) [29] and TimeSformer [1], to extract local spatio-temporal information.

In general, an effective temporal modeling module assists the model in extracting long-term dependencies and perceiving temporal distortions in videos. Existing models usually perform temporal modeling on concatenated features and do not fully exploit the gaps in representing video quality over time among different features. Based on the analysis of Figure 1(b), we propose the CATM module to perceive the temporal content variation and quality saliency information of the video, which fully considers the temporal characteristics of two aware features in videos with varying quality.

3 PROPOSED METHOD

Figure 2 depicts the framework of the proposed semantic-aware and quality-aware interaction network (**A^{2}INet**) for BVQA. The distorted video is first inputted into a feature extraction module to extract spatial quality-aware and semantic-aware features (Section 3.1). Subsequently, the cross-aware guided interaction (CAGI) module is employed to perceive local perceptual gaps between the two aware features and achieve global interaction (Section 3.2). Next, the fused features are fed into a cross-aware temporal modeling (CATM) module to further capture quality-aware and semantic-aware long-term dependencies, and aggregate frame-level features through temporal pooling to estimate the video-level quality score (Section 3.3). Each module is introduced in detail below.

3.1 Feature Extraction

Based on previous subjective experiments regarding human preferences in visual quality [43, 47, 48], we extract spatial quality-aware features and spatial (or motion) semantic-aware features to represent video quality. The proposed model is designed a dual-branch architecture, comprising a quality-aware network and a semantic-aware network, for extracting two aware features. A distorted video $\mathcal{V} = \{\mathcal{V}(h, w, t)\} \in \mathbb{R}^{H \times W \times T}$ is treated as a collection of frame-level images, where $H \times W$ represents the spatial resolution of the video, and T is the video length.

We employ an IQA model [57] pre-trained on multiple IQA datasets as the quality-aware network. Given that the visual perception system is a hierarchical structure [27, 49], features $\boldsymbol{F}_t^{q1} \in \mathbb{R}^{64\times \frac{H}{2} \times \frac{W}{2}}$, $\boldsymbol{F}_t^{q2} \in \mathbb{R}^{128\times \frac{H}{4} \times \frac{W}{4}}$, $\boldsymbol{F}_t^{q3} \in \mathbb{R}^{256\times \frac{H}{8} \times \frac{W}{8}}$ and $\boldsymbol{F}_t^{q4} \in \mathbb{R}^{512\times \frac{H}{16} \times \frac{W}{16}}$ are extracted from four bottlenecks of the quality-aware network, where t represents the t-th frame. Then, the spatial global average pooling and global standard deviation pooling are applied for the features of each bottleneck. The pooled features are concatenated into features $\boldsymbol{f}_t^q \in \mathbb{R}^{1\times 1920}$ at the t-th frame, and the quality-aware features of the distorted video are represented as features $\boldsymbol{F}^q = \left\{\boldsymbol{f}_t^q\right\} \in \mathbb{R}^{T\times 1920}$.

For the other branch, we use the pre-trained ResNet-50 [13] on the ImageNet dataset [7] as the semantic-aware network. Similarly, we extract semantic-aware features from the distorted video, denoted as $\boldsymbol{F}^s = \left\{\boldsymbol{f}_t^s\right\} \in \mathbb{R}^{T\times 7680}$. To align the feature dimensions of the two aware features, we pass the features both through a fully connected (FC) layer and obtain features $\boldsymbol{F}_f^s$ and $\boldsymbol{F}_f^q \in \mathbb{R}^{T\times D}$.

3.2 Cross-aware Guided Interaction Module

We propose the CAGI, which comprises a cross-aware guided instance normalization (CGIN) and a global self-attention layer, to perceive local gaps and achieve global interaction between features.

1) CGIN. An adaptive instance normalization is proposed for style transfer [16] by combining the mean and variance of the features from content image $\boldsymbol{I}_X$ with the features from style image

I_Y, which is defined as

$$\mathrm{AdaIN}\left(X, Y\right) = \sigma\left(Y\right) \frac{X - \mu\left(X\right)}{\sigma\left(X\right)} + \mu\left(Y\right) \quad (1)$$

where X and $Y \in \mathbb{R}^{B \times C \times H \times W}$ are the features of input images I_X and I_Y respectively, B, C, H, and W represent the batch size, the feature channel, the height, and width of feature map, respectively, $\mu(\cdot)$ and $\sigma(\cdot)$ calculate across spatial dimensions independently for each channel and each sample of X and Y [10, 30].

Inspired by this module, we use feature guided instance normalization (FGIN) to interact the cross-aware features,

$$\mathrm{FGIN}\left(X, Y\right) = \gamma_s\left(Y\right) \frac{X - \mu\left(X\right)}{\sigma\left(X\right)} + \theta_s\left(Y\right) \quad (2)$$

where $\gamma_s(\cdot)$ and $\theta_s(\cdot)$ denote both an FC layer, $\gamma_s(Y)$ and $\theta_s(Y)$ are treated as affine parameters to scale and shift the normalized features X, thereby facilitating the interaction between the two features. However, the process of deforming X to Y by Eq. (2) leads to the loss of the original information of X. For this reason, we further modify Eq. (2), as follows

$$f\left(X, Y\right) = \gamma_s\left(Y\right) \frac{X - \mu\left(X\right)}{\sigma\left(X\right)} + \theta_s\left(Y\right) + \gamma_1 \frac{X - \mu\left(X\right)}{\sigma\left(X\right)} \quad (3)$$

where γ_1 is a constant and is set to 1. As shown in Eq. (3), we add normalized features X in Eq. (3), which prevents the network from losing information X during feed-forward. Finally, the proposed CGIN is formulated as follows,

$$\mathrm{CGIN}\left(F_f^q, F_f^s\right) = f\left(F_f^q, F_f^s\right) \oplus f\left(F_f^s, F_f^q\right) = F^{qs} \oplus F^{sq} \quad (4)$$

We narrow the perceptual gaps between the cross-aware features by deforming them towards each other, and then concatenate F^{qs} and F^{sq} to form the feature $F^{pe} \in \mathbb{R}^{T \times 2D}$.

2) Global self-attention layer. After perceiving local gaps on cross-aware features, a global self-attention layer [42, 50] is designed to enhance the global interaction between frames.

Similar to the self-attention mechanism, the feature F^{pe} generates query F_Q^{pe}, key F_K^{pe} and value $F_V^{pe} \in \mathbb{R}^{T \times 2D}$ matrices through three linear projections W_Q, W_K and $W_V \in \mathbb{R}^{2D \times 2D}$ to encode temporal information of the F^{pe},

$$F_{am}^{pe} = M_{softmax}\left(\frac{F_Q^{pe}\left(F_K^{pe}\right)^{\mathrm{T}}}{\sqrt{2D}}\right) \in \mathbb{R}^{T \times T} \quad (5)$$

where $M_{softmax}(\cdot)$ means a Softmax function, "T" represents the transpose operator. The values of F_{am}^{pe} reflect the correlation of two elements between frames. Finally, the F_{am}^{pe} is directly multiplied by the F_V^{pe}, and F^{pe} with residual links [42] is added to obtain the feature F^e.

3.3 Cross-aware Temporal Modeling

The CATM module is designed to capture temporal distortions associated with video quality degradation and to regress features into video-level quality scores.

Previous research has shown that frames with severe quality degradation may have a greater impact on the quality of the whole video [54]. Additionally, factors such as camera shake and scene transitions [46] also influence video quality. By integrating these

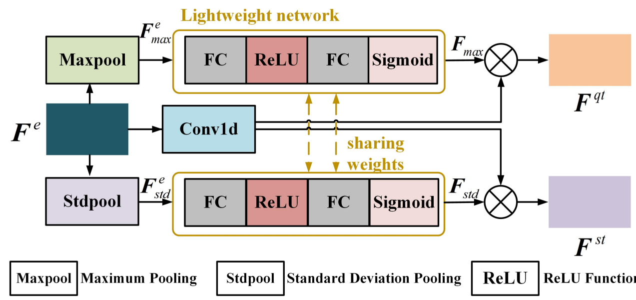

Figure 3: Illustrations of the quality saliency perception and content variation perception blocks.

theoretical findings with the insights from Figure 1, we develop the quality saliency perception and content variation perception blocks to enhance the perception of temporal quality, as depicted in Figure 3. Before input to the CATM module, feature F^e is reduced to the D-dimension through an FC layer, and maximum pooling and standard deviation pooling are utilized to aggregate the saliency and variation information of feature F^e along the temporal dimension. Subsequently, features F_{max}^e and $F_{std}^e \in \mathbb{R}^{1 \times D}$ are fed into a lightweight network that consists of two FC layers, one ReLU function and one Sigmoid function to obtain features F_{max} and F_{std}. Then, F^e is multiplied by F_{max} and F_{std} after passing through a temporal convolution layer to derive the temporal quality saliency and content variation information, respectively. Finally, F^{qt} and F^{st} are concatenated into $F^z \in \mathbb{R}^{T \times 2D}$ and input to the temporal network to build long-term dependencies.

Similar to previous work [23], we first crop the feature F^z by using a FC layer, and the reduced feature $\tilde{F}^z = \left\{\tilde{f}_t^z\right\} \in \mathbb{R}^{T \times 128}$ is obtained. Then, the feature $\tilde{F}^z$ is input into GRUs to capture long-term dependencies. And a FC layer is used to regress the output features $H_t = \{h_t\} \in \mathbb{R}^{T \times 32}$ of GRUs into frame-level scores $q = \{q_t\} \in \mathbb{R}^{T \times 1}$. We adopt a subjectively-inspired temporal pooling strategy [36] to integrate frame-level scores q to a video-level score Q^p.

3.4 Sampling Strategy and Optimization

1) Sampling strategy. Existing fixed backbone-based methods usually extract features for full-resolution videos, resulting in models with high complexity that increases with the resolution of the video. In this end, we propose a simple video sampling strategy based on the characteristics of semantic-aware features and quality-aware features to balance the effectiveness and efficiency of the models. On one hand, as observed from Figure 1(a), semantic-aware features focus on object and contextual semantics but has little effect on quality degradation. On the other hand, quality-aware features are sensitive to local quality degradation but lacks understanding of global semantic content. Thus, we resize each frame to preserve the original global semantics and randomly crop each frame into four 768×768 patches to ensure the original local quality. The resized frame is set to $min\left(H, W\right) = 540$ while maintaining the aspect ratio, and we strictly aligned the sample areas to ensure raw temporal variations during patch sampling [18, 44], where $min(\cdot)$

denotes the minimum operation. Finally, the imresized video and the cropped video are fed into the semantic-aware and quality-aware networks, respectively. And, the features of four patches are averaged as frame-level quality-aware features.

2) Optimization. During training, the proposed model is optimized using mean absolute error (MAE) loss $\mathcal{L}_M$ and rank loss $\mathcal{L}_R$ as objective functions. The MAE loss measures the distance between the predicted score Q^p and the mean opinion score (MOS) Q^m, denoted as:

$$\mathcal{L}_M = \frac{1}{B}\sum_{i=1}^{B}\left|Q_i^p - Q_i^m\right| \tag{6}$$

where i represents the i-th video from the mini-batch. The differentiable rank loss function is calculated as:

$$\mathcal{L}_R = \frac{1}{B^2}\sum_{i=1}^{B}\sum_{j=1}^{B}\max\left(0, \left|\bar{Q}_{ij}^m\right| - \phi\left(Q_i^m, Q_j^m\right)\left(\bar{Q}_{ij}^p\right)\right) \tag{7}$$

where $\bar{Q}_{ij}^s = Q_i^s - Q_j^s$, $s \in \{m, p\}$, and $\phi(\cdot)$ is defined as :

$$\phi\left(Q_i, Q_j\right) = \begin{cases} 1, & \text{if } Q_i \geq Q_j \\ -1, & \text{if } Q_i < Q_j \end{cases} \tag{8}$$

Finally, the training loss function is represented by:

$$\mathcal{L}_{INet} = \mathcal{L}_{MAE} + \eta\mathcal{L}_{rank} \tag{9}$$

where η is the parameter used to balance the two losses.

4 EXPERIMENTS

4.1 Experimental Settings

1) Implementation details. In the experiment, the dimension parameter D is set to 1024, and the balance parameter η is set to 1. During training, we freeze the weights of the quality- and semantic-aware networks. To compare with the VQA model based on the 3D network, we replace the spatial semantic-aware network with the SlowFast [9] pre-trained on the action recognition dataset [2] as the motion semantic-aware network. Only the fast features from the last layer of the network are used as motion semantic features, with the feature dimension of $\boldsymbol{F}^s$ being 512. As a distinction, we use **S+S** to represent the combination of spatial quality-aware and spatial semantic-aware, and **S+M** to represent the combination of spatial quality-aware and motion semantic-aware. Moreover, we set up two video input modes, full resolution and preprocessing, which are abbreviated as **Proposed FR** and **Proposed PR**. For **Proposed FR**, we take the whole video as the input. For **Proposed PR**, we sample 128 frames from the video at the same interval and process them as input by the preprocessing described in Section 3.4. The experiments are conducted on PyTorch [34] with single RTX 3090 GPU. The batch size is set to 8, and Adam optimizer with an initial learning rate of 2×10^{-5} is used for training learnable parameters.

2) Compared methods. The performance of the proposed model is compared with sixteen VQA models, including two models combining hand-crafted and deep features (RAPIQUE [41] and CNN-VQM [20]), and fourteen deep learning-based VQA models (including eight fixed backbone models, VSFA [23], GSTVQA [3], CoINVQ [43], PVQ [52], DCVQE [26], Li *et al.* [22], CONVIQT [31] and HVS-5M [56], and six end-to-end training models, FAST-VQA [44], SimpleVQA [38], FasterVQA [45], ZoomVQA [59], DisCoVQA [46] and VQT [55]). Note that all models are run with the source code released by the authors and are not trained with additional VQA datasets. Two RTX 3090 GPUs are used for training HVS-5M [56], FAST-VQA [44], FasterVQA [45], ZoomVQA [59] and SimpleVQA [38].

Table 1: Summary of six benchmark VQA datasets used for experiments. These datasets cover videos with various scenes, resolutions, durations and frame rates, which can test the performance of models on various videos. "Num. Videos", "Num. Frames", "Spatial Res." and "Time Dur." mean the number of videos,the number of frames, spatial resolution and time duration, respectively.

Dataset	Num. Videos	Spatial Res.	Num. Frames	Time Dur.	MOS Range
CVD2014 [33]	234	480p,720p	[143,830]	10-25s	[-6.5,93.4]
LIVE-Qual [11]	208	1080p	[358,526]	15s	[16.6,73.6]
LIVE-VQC [37]	585	240p-1080p	[166,1202]	10s	[6.2,94.3]
YT-UGC [43]	1142	360p-4k	[71,600]	20s	[1.2,4.7]
KoNViD-1k [14]	1200	540p	[181,240]	8s	[1.2,4.6]
LSVQ [52]	38811	99p-4k	[15,605]	5-12s	[2.4,91.4]

3) Six benchmark VQA datasets. Six VQA datasets with mean opinion scores (MOS) are used as benchmark datasets to test the performance of different models, including **five small-scale** datasets (CVD2014 [33], LIVE-Qual [11], LIVE-VQC [37], YT-UGC [43] and KoNViD-1k [14]) and **one large-scale** dataset (LSVQ [52]), their details are listed in Table 1. The LSVQ dataset comprises a train subset ($\text{LSVQ}_{\text{train}}$), and two test subsets ($\text{LSVQ}_{\text{test}}$ and $\text{LSVQ}_{\text{1080p}}$), containing 28056, 7182 and 3573 videos, respectively. For YT-UGC dataset, we follow [22] and 1142 videos are selected for experiments.

4) Evaluation criteria. For each VQA dataset, we follow the settings of [38, 44] and the videos in each dataset are partitioned into training and test sets. Specifically, we train each model on the training set and verify the performance of the model on the test set. Pearson linear correlation coefficient (PLCC) and Spearman rank-order correlation coefficient (SRCC) are used as evaluation criteria to quantify the correlation between predicted scores and subjective judgments (*i.e.*, MOS values), where SRCC reflects the monotonicity of BVQA models, and PLCC is utilized to evaluate the accuracy of BVQA models. Following [12], a nonlinear logistic function maps the predicted scores to the same scale as the MOS before calculating PLCC. The train-test splits are repeated ten times to avoid performance bias, and the median results are reported.

4.2 Comparison on Individual Datesets

Table 2 presents the comparison results of the proposed models and sixteen BVQA models on five small-scale datasets. In Table 2, the weighted performance of the **proposed FR(S+M)** model surpasses that of the SOTA model [56] by **2.91%** and **3.39%** in terms of PLCC and SRCC, respectively. The **proposed FR(S+M)** model outperforms prior fixed backbone methods on four small-scale datasets, achieving **7.25%**, **2.43%**, **4.92%** and **3.95%** improvements over the second-best results in terms of SRCC on the LIVE-Qual, CVD2014, LIVE-VQC, and KoNViD-1k datasets. It is worth mentioning that the **proposed FR(S+S)** model, which does not consider local spatio-temporal information, still shows competitiveness. The

Table 2: Results on the five benchmark VQA datasets. "F" and "B" represent feature type and backbone network, "H" and "D" stand for hand-crafted and deep features, "2D" and "3D" denote 2D and 3D backbone networks. "W.A." shows the weighted-average performance over all datasets, and weights are proportional to database-sizes. The best and second best results for fixed backbone methods are highlighted in red bold and blue bold respectively. The best result for end-to-end training methods is underlined. *Italics* indicate data sourced from original references. "-" indicates that the results are not available.

Type	Models	F	B	LIVE-Qual (208)		CVD2014 (234)		LIVE-VQC (585)		YT-UGC (1142)		KoNViD-1k (1200)		W.A. (3369)	
				PLCC	SRCC	PLCC	SRCC	PLCC	SRCC	PLCC	SRCC	PLCC	SRCC	PLCC	SRCC
Fixed-Backbone	CNN+TLVQM(MM,20)	H+D	2D	0.8278	0.8220	0.7795	0.7486	0.8037	0.7719	0.8225	0.8112	0.8278	0.8220	0.8185	0.8045
	RAPIQUE(OJSP,21)	H+D	2D	0.7325	0.6927	0.7174	0.7177	0.7626	0.7879	0.7510	0.7429	0.8143	0.8060	0.7721	0.7683
Fixed-Backbone	VSFA(MM,19)	D	2D	0.8007	0.7671	0.8735	0.8732	0.7889	0.7255	0.7737	0.7659	0.7951	0.7943	0.7926	0.7765
	GSTVQA(TCSVT,21)	D	2D	0.7544	0.6873	0.8783	0.8718	0.7429	0.7260	0.7714	0.7758	0.8091	0.8133	0.7863	0.7817
	CoINVQ(CVPR,21)	D	2D+3D	-	-	-	-	-	-	*0.802*	*0.816*	*0.764*	*0.767*	-	-
	PVQ(CVPR,21)	D	2D+3D	-	-	-	-	*0.837*	*0.827*	-	-	*0.791*	*0.786*	-	-
	DCVQE(ACCV,22)	D	2D	0.5822	0.7073	0.7601	0.8296	0.6316	0.7282	0.6599	0.7739	0.7953	0.8024	0.7054	0.7759
	Li *et al*(TCSVT,22)	D	2D+3D	0.8253	0.8150	0.9043	0.8909	0.8441	0.8515	0.8237	0.8387	0.8473	0.8514	0.8413	0.8476
	CONVIQT(TIP,23)	D	2D	*0.802*	*0.797*	*0.837*	*0.858*	*0.817*	*0.808*	*0.822*	*0.832*	*0.849*	*0.851*	*0.831*	*0.834*
	HVS-5M(TCYB,23)	D	2D+3D	0.8218	0.7866	0.8903	0.8780	0.8470	0.8531	0.8490	0.8519	0.8536	0.8538	0.8515	0.8506
End-to-End	FAST-VQA(ECCV,22)	D	3D	0.8053	0.8093	0.8727	0.8635	0.7950	0.7515	0.8102	0.8122	0.8547	0.8489	0.8275	0.8181
	SimpleVQA(MM,22)	D	2D+3D	0.8304	0.8054	0.8987	0.8836	0.8329	0.7907	0.7915	0.7971	0.8521	0.8483	0.8301	0.8208
	Faster-VQA(TPAMI,23)	D	3D	0.7480	0.7477	0.8564	0.8490	0.8133	0.7690	0.8135	0.7987	0.8534	0.8500	0.8266	0.8122
	DisCoVQA(TCSVT,23)	D	3D	*0.823*	*0.825*	*0.893*	*0.897*	*0.844*	*0.838*	-	-	*0.860*	*0.863*	-	-
	ZoomVQA(CVPR,23)	D	2D+3D	0.8222	0.7987	0.8926	0.8719	0.7677	0.7227	0.8346	0.8409	0.8280	0.8301	0.8239	0.8161
	VQT(MM,23)	D	3D	-	-	-	-	*0.8357*	*0.8238*	*0.8514*	*0.8357*	*0.8684*	*0.8582*	-	-
Fixed-Backbone	**Proposed PR(S+S)**	D	2D+2D	0.8785	0.8573	**0.9182**	**0.9059**	0.8493	0.8184	0.8472	**0.8536**	0.8657	0.8669	0.8610	0.8561
	Proposed FR(S+S)	D	2D+2D	0.8764	**0.8676**	**0.9183**	0.9056	0.8484	0.8195	**0.8530**	0.8531	0.8668	0.8695	0.8631	0.8577
	Proposed PR(S+M)	D	2D+3D	**0.8860**	0.8656	0.9128	0.9042	**0.8894**	**0.8869**	0.8408	0.8478	**0.8785**	**0.8850**	**0.8705**	**0.8729**
	Proposed FR(S+M)	D	2D+3D	**0.8865**	**0.8741**	0.9144	**0.9126**	**0.8952**	**0.8951**	**0.8518**	**0.8569**	**0.8812**	**0.8875**	**0.8763**	**0.8794**

proposed FR(S+S) model improves the LIVE-Qual, CVD2014 and KoNViD-1k datasets by **6.45%**, **1.65%** and **1.84%** in terms of SRCC, respectively. One possible reason for the weaker performance of the **proposed FR(S+S)** model on the LIVE-VQC dataset is that local spatio-temporal information plays a significant role in this dataset. Despite freezing the feature extractors, the weighted performance of our proposed models still outperforms that of all end-to-end training methods. In summary, the proposed model achieves SOTA performance by analyzing domain gaps across aware features and enhancing the perception of two aware features in space and time through CAGI and CATM, rather than directly concatenating features. Furthermore, the weighted performance of the **proposed PR** models is only slightly lower than that of the **proposed FR** models. We will further compare their complexity in Section 4.6.

In addition to analyzing the superior performance of the proposed model, we draw several other conclusions. First, the performance of models based on 3D feature extractors is superior to that of models based on 2D feature extractors, suggesting that local spatio-temporal information is more crucial than spatial features for VQA tasks. Although models [3, 23, 26] temporally model frame-level features via temporal network, the separate extraction of spatial and temporal features fails to capture intrinsic spatio-temporal information. Second, models based on multiple feature extractors outperform those based on a single feature extractor. The utilization of multiple feature extractors enables the capture of various perceptual features, providing a richer representation for video quality degradation and yielding superior performance. Lastly, the performance of fixed backbone-based methods is comparable to that of end-to-end training methods in small-scale datasets. End-to-end training-based methods fine-tune the backbone network to extract features related to visual quality while using only part of the video data (clips or sparse frames) as input. Fixed backbone-based methods use feature extractors pre-trained from other tasks, yet they have access to more comprehensive video data. As a result, both methods have similar prediction performance on small datasets.

4.3 Intra- and Cross-dataset Validation

Next, we conduct intra- and cross-dataset validation to verify the generalization ability of the proposed model. The models are trained on the $\text{LSVQ}_{\text{train}}$ subset and validated on the $\text{LSVQ}_{\text{test}}$ and $\text{LSVQ}_{\text{1080p}}$ (intra-dataset validation). For cross-dataset validation, the optimal trained model is tested on LIVE-VQC and KoNViD-1k datasets. We choose VSFA [23] GSTVQA [3], PVQ [52], Li *et al* [22], CONVIQT [31] and HVS-5M [56] as comparison models, as they freeze the backbone network during training. Table 3 presents the comparative results. The **proposed PR(S+M)** and **FR(S+M)** models have better generalization performance. Although the **proposed FR(S+M)** model has poor cross-dataset validation performance on the LIVE-VQC dataset, it demonstrates excellent performance in both intra- and cross-dataset validation. The **proposed PR(S+S)** and **FR(S+S)** models outperform all VQA models based on the 2D backbone network, and even surpass PVQ [52], which includes a 3D feature extractor. The performance of the **proposed PR(S+S)** even outperforms the **proposed FR(S+S)** with performance by training on a large amount of video data on the $\text{LSVQ}_{\text{test}}$ dataset. Overall, the proposed models have good generalization performance.

4.4 Qualitative Results

To illustrate the correlation between predicted scores with subjective scores (*i.e.* MOS), we first visualize the scatter plots of the

Table 3: Results of the intra- and cross-dataset validation on $\text{LSVQ}_{\text{test}}$, $\text{LSVQ}_{\text{1080p}}$, and two small-scale datasets. The best and second results are highlighted in red bold and blue bold.

Models	Intra-dataset				Cross-dataset			
	$\text{LSVQ}_{\text{test}}$		$\text{LSVQ}_{\text{1080p}}$		KoNViD-1k		LIVE-VQC	
	PLCC	SRCC	PLCC	SRCC	PLCC	SRCC	PLCC	SRCC
VSFA	0.8050	0.8045	0.7201	0.6803	0.8174	0.8163	0.7896	0.7459
GSTVQA	0.7983	0.7985	0.7053	0.6754	0.7998	0.7954	0.7604	0.7057
PVQ	*0.828*	*0.827*	*0.739*	*0.711*	*0.795*	*0.791*	*0.807*	*0.770*
Li *et al.*	0.8567	0.8574	0.7825	0.7695	0.8379	0.8369	0.8136	0.7892
CONVIQT	0.820	0.821	-	-	-	-	-	-
HVS-5M	0.8702	0.8731	**0.8099**	**0.7830**	0.8445	0.8401	**0.8249**	0.8013
Proposed PR(S+S)	0.8564	0.8561	0.7849	0.7420	0.8446	0.8375	0.8068	0.7574
Proposed FR(S+S)	0.8539	0.8542	0.7799	0.7331	0.8341	0.8329	0.7896	0.7509
Proposed PR(S+M)	**0.8805**	**0.8789**	0.8063	0.7741	**0.8598**	**0.8640**	**0.8391**	**0.8082**
Proposed FR(S+M)	**0.8779**	**0.8780**	**0.8182**	**0.7851**	**0.8640**	**0.8673**	0.8154	**0.8165**

proposed FR (S+S) and **PR (S+M)** models on the $\text{LSVQ}_{\text{test}}$ dataset in Figure 4. We observe that most of **the scatter points** cluster around **the red line**, indicating that the scores predicted by the models are consistent with the subjective scores.

Then, we further demonstrate one successful and one failed video prediction case of the **proposed FR (S+M)** model in Figure 5. The proposed model accurately predicts video scenes with obvious semantic information but fails to predict video examples where the semantic content is not apparent. One possible explanation is that the proposed method utilizes a fixed backbone network to extract semantic features and relies on the presence of specific semantic scenarios. Overall, the quantitative results illustrate the effectiveness of the proposed model and provide inspirations for us to better handle these scenarios in the future.

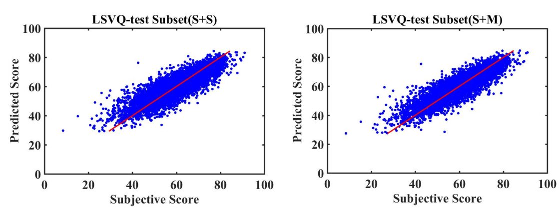

(a) (b)

Figure 4: Scatter plots of predicted scores on the $\text{LSVQ}_{\text{test}}$ dataset by (a) the proposed FR (S+S) model and (b) the proposed FR (S+M) model.

(a) (b)

Figure 5: (a) The one successful and (b) one failure prediction cases of the proposed FR (S+M) model.

4.5 Ablation Studies

In this section, the whole video is utilized as input for ablation experiments to assess the effectiveness of each module.

Ablation on quality-aware and semantic-aware features. To quantitatively analyze the independent performance and mutual gains of quality-aware and semantic-aware features, we report the PLCC and SRCC results of spatial quality-aware, spatial semantic-aware, motion semantic-aware features and their combinations in Table 4. Note that all features are fed directly into a temporal network and a temporal pooling as described in Section 3.3. First, we found that the quality-aware feature typically takes a prominent role in VQA. Second, combining different aware features brings gains and improves the prediction performance of the model. Moreover, the combinations of quality-aware with semantic-aware (spatial or motion) yield superior results compared to combining two semantic-aware features, owing to the fact that they have more complementary information in distorted videos.

Table 4: Ablation experiments on spatial quality-aware (SQ), spatial semantic-aware (SS), motion semantic-aware (MS) features and combinations (+) using three small-scale datasets. We have respectively bolded the best-performing features and combinations.

Feat ures	LIVE-Qual		LIVE-VQC		KoNViD-1k	
	PLCC	SRCC	PLCC	SRCC	PLCC	SRCC
SQ	**0.8179**	**0.7764**	**0.8040**	**0.7599**	**0.8224**	**0.8261**
SS	0.8099	0.7697	0.7918	0.7317	0.8156	0.8049
MS	0.6590	0.6159	0.7814	0.7372	0.7109	0.6993
SQ+SS	0.8193	**0.8031**	0.8124	0.7750	0.8390	0.8435
SQ+MS	**0.8207**	0.7986	**0.8546**	**0.8526**	**0.8465**	**0.8499**
SS+MS	0.8047	0.7728	0.8448	0.8396	0.8287	0.8278

Ablation on CAGI module. We compare three schemes that combine quality-aware features with semantic-aware features, including direct concatenation (Concat), concatenation followed by multilayer perceptron fusion (Concat+MLP), and the CAGI module. Among them, the MLP consists of an FC layer, ReLU function, and dropout layer. Then, the fused features are input into an FC layer and a temporal network as described in Section 3.3. For a full comparison, we use variants of the CNN and Transformer architectures to extract each perceptual feature and compose eight quality-semantic aware combinations for analysis. Table 5 presents the performance comparison of the three schemes. Intuitively, we observe that each feature combination through CAGI exhibits higher performance than direct concatenation and is more efficient than simple MLP fusion, proving that CAGI effectively enhances the correlation between the two aware features. Furthermore, CAGI is compatible for most dual-branch architectures.

Ablation on CGIN. We further investigate the impact of three instance normalizations on the proposed model, including adaptive instance normalization (AdaIN) [16], feature guided instance normalization (FGIN) [10], and the proposed CGIN. The comparison results are listed in Table 6. From Table 6, we observe that the proposed CGIN obtains higher prediction accuracy, which implies that CGIN is more helpful for the interaction of two aware features.

Table 5: Performance comparison results using concatenation (Concat), concatenation followed by multi-layer perceptron fusion (Concat+MLP) and CAGI module combining the two aware features. We use varients of the CNN [9, 13, 57] and Transformer (ViT) [8, 29, 50] pre-trained on IQA, image classification and action recognition datasets, respectively, as backbone networks to extract spatial quality aware (CNN and ViT), spatial semantic aware (CNN and ViT), and motion semantic-aware (Fast and Swin) features. Blue and red fonts indicate quality-aware and semantic-aware features, respectively, and the performance gains of Concat+MLP and CAGI module are highlighted in green and purple.

Module	LIVE-VQC								KoNViD-1k							
	CNN+CNN	CNN+ViT	CNN+Fast	CNN+Swin	ViT+CNN	ViT+ViT	ViT+Fast	ViT+Swin	CNN+CNN	CNN+ViT	CNN+Fast	CNN+Swin	ViT+CNN	ViT+ViT	ViT+Fast	ViT+Swin
Concat	0.7750	0.7879	0.8526	0.7920	0.7824	0.7714	0.8438	0.7868	0.8435	0.8290	0.8499	0.8334	0.8405	0.8114	0.8486	0.8179
Concat+MLP	0.7810	0.8061	0.8698	0.8087	0.7907	0.7823	0.8536	0.7871	0.8411	0.8362	0.8694	0.8340	0.8445	0.8331	0.8582	0.8190
Improvement	**0.77%**	**2.31%**	**2.01%**	**2.11%**	**1.06%**	**1.41%**	**1.16%**	**0.04%**	**-0.28%**	**0.87%**	**2.29%**	**0.07%**	**0.48%**	**2.67%**	**1.13%**	**0.13%**
CAGI	0.8159	0.8423	0.8840	0.8377	0.8264	0.8276	0.8826	0.8302	0.8665	0.8697	0.8751	0.8645	0.8584	0.8574	0.8597	0.8548
Improvement	**5.28%**	**6.90%**	**3.68%**	**5.77%**	**5.62%**	**7.29%**	**4.60%**	**5.52%**	**2.73%**	**4.91%**	**2.97%**	**3.73%**	**2.13%**	**5.67%**	**1.31%**	**4.51%**

Table 6: SRCC results of different instance normalization, where "S" and "Q" mean semantic- and quality-aware features, "S→Q" represents the deformation of feature S to feature Q. The best results are bolded.

Module		LIVE-Qual (S+S)	LIVE-Qual (S+M)	LIVE-VQC (S+S)	LIVE-VQC (S+M)	KoNViD-1k (S+S)	KoNViD-1k (S+M)
AdaIN	S→Q	0.8513	0.7915	0.7824	0.8774	0.8514	0.8658
	Q→S	0.8442	0.8508	0.7642	0.8727	0.8537	0.8715
FGIN	S→Q	0.8485	0.8611	0.7914	0.8820	0.8583	0.8750
	Q→S	0.8398	0.8658	0.7897	0.8794	0.8587	0.8776
CGIN		**0.8676**	**0.8741**	**0.8195**	**0.8951**	**0.8695**	**0.8875**

Table 7: Ablation on each component of the proposed model using three VQA datasets. We choose the VSFA [23] model as our baseline. Each component improves the performance of the model. The best results are bolded.

Model	FE	GC	TM	LIVE-Qual PLCC	LIVE-Qual SRCC	LIVE-VQC PLCC	LIVE-VQC SRCC	KoNViD-1k PLCC	KoNViD-1k SRCC
Baseline	✓	×	×	0.8007	0.7671	0.7889	0.7255	0.7951	0.7943
Proposed (S+S)	✓	×	×	0.8193	0.8031	0.8124	0.7750	0.8390	0.8435
	✓	✓	×	0.8657	0.8587	0.8390	0.8159	0.8628	0.8665
	✓	✓	✓	**0.8764**	**0.8676**	**0.8484**	**0.8195**	**0.8668**	**0.8695**
Proposed (S+M)	✓	×	×	0.8207	0.7986	0.8546	0.8526	0.8465	0.8499
	✓	✓	×	0.8785	0.8653	0.8905	0.8840	0.8711	0.8751
	✓	✓	✓	**0.8865**	**0.8741**	**0.8952**	**0.8951**	**0.8812**	**0.8875**

Ablation on each component of the proposed model. We investigate the effectiveness of each module, including the feature extraction module (FE), the CAGI module (GI), and the CATM module (TM). Table 7 lists the performance results of different model designing on three datasets. Based on the qualitative and quantitative analysis of the two aware features, we meticulously designed each module, and Table 7 proves that each module has certain gains for the proposed model.

4.6 Computational Complexity

In this subsection, we compare the FLOPs and running times on GPU of the proposed models with existing models, and plot the performance curves of FLOPs and running times on videos with different resolutions in Figure 6. Average results of ten video samples (10 seconds, 30 frames per second) as final test time, and experiments are executed on a single 3090 GPU. It can observe that the FLOPs and running time of the existing models increase with the rise in video resolution. Although HVS-5M [56] exhibits good prediction performance, the computational complexity is unacceptable. When video resolution exceeded 540P, the HVS-5M run for more than 100s and 2160P video could not be tested on a single 3090 GPU (540P, 134.54s; 720P, 224.08s; 1080P, 388.82s; 1440P, 687.7s). The **proposed FR(S+S)** and **FR(S+M)** models achieve SOTA performance with computational complexity between VSFA [23] and GSTVQA [3]. The **proposed PR(S+S)** and **PR(S+M)** models reduce redundant information from the input video through a simple sampling strategy (as described in Section 3.4), achieving the lowest computational complexity while maintaining performance with the whole video as input (see Table 2).

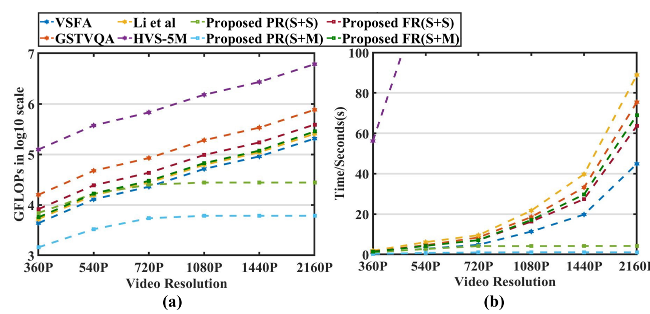

Figure 6: (a) FLOPs and (b) running time performance curves of the proposed models and four models on videos with different resolutions.

5 CONCLUSION

In this paper, we have presented the semantic-Aware and quality-Aware Interaction Network (**A^{2}INet**) for blind video quality assessment (BVQA). Based on the analysis of the domain gaps between semantic- and quality-aware features, we design a cross-aware guided interaction module to enhance the interaction between the two aware features and propose a cross-aware temporal modeling module to perceive temporal distortion from the perspectives of content variation and quality saliency. Experimental results show that the proposed model outperforms the state-of-the-art performance on six benchmark VQA datasets, and ablation studies further verify the effectiveness of each component. Additionally, we demonstrate a simple video sampling strategy to balance the effectiveness and efficiency of the proposed model.

REFERENCES

[1] Gedas Bertasius, Heng Wang, and Lorenzo Torresani. 2021. Is space-time attention all you need for video understanding?. In *International Conference on Machine Learning*, Vol. 2. 4.

[2] Joao Carreira and Andrew Zisserman. 2017. Quo vadis, action recognition? a new model and the kinetics dataset. In *Proceedings of the IEEE Conference on Computer Vision and Pattern Recognition*. 6299–6308.

[3] Baoliang Chen, Lingyu Zhu, Guo Li, Fangbo Lu, Hongfei Fan, and Shiqi Wang. 2021. Learning generalized spatial-temporal deep feature representation for no-reference video quality assessment. *IEEE Transactions on Circuits and Systems for Video Technology* 32, 4 (2021), 1903–1916.

[4] Pengfei Chen, Leida Li, Lei Ma, Jinjian Wu, and Guangming Shi. 2020. RIRNet: Recurrent-in-recurrent network for video quality assessment. In *Proceedings of the 28th ACM International Conference on Multimedia*. 834–842.

[5] Kyunghyun Cho, Bart Van Merriënboer, Caglar Gulcehre, Dzmitry Bahdanau, Fethi Bougares, Holger Schwenk, and Yoshua Bengio. 2014. Learning phrase representations using RNN encoder-decoder for statistical machine translation. *arXiv preprint arXiv:1406.1078* (2014).

[6] Sathya Veera Reddy Dendi and Sumohana S Channappayya. 2020. No-reference video quality assessment using natural spatiotemporal scene statistics. *IEEE Transactions on Image Processing* 29 (2020), 5612–5624.

[7] Jia Deng, Wei Dong, Richard Socher, Li-Jia Li, Kai Li, and Li Fei-Fei. 2009. Imagenet: A large-scale hierarchical image database. In *Proceedings of the IEEE/CVF Conference on Computer Vision and Pattern Recognition*. 248–255.

[8] Alexey Dosovitskiy, Lucas Beyer, Alexander Kolesnikov, Dirk Weissenborn, Xiaohua Zhai, Thomas Unterthiner, Mostafa Dehghani, Matthias Minderer, Georg Heigold, Sylvain Gelly, et al. 2020. An Image is Worth 16x16 Words: Transformers for Image Recognition at Scale. In *International Conference on Learning Representations*.

[9] Christoph Feichtenhofer, Haoqi Fan, Jitendra Malik, and Kaiming He. 2019. Slowfast networks for video recognition. In *Proceedings of the IEEE/CVF International Conference on Computer Vision*. 6202–6211.

[10] Yuqian Fu, Li Zhang, Junke Wang, Yanwei Fu, and Yu-Gang Jiang. 2020. Depth guided adaptive meta-fusion network for few-shot video recognition. In *Proceedings of the 28th ACM International Conference on Multimedia*. 1142–1151.

[11] Deepti Ghadiyaram, Janice Pan, Alan C Bovik, Anush Krishna Moorthy, Prasanjit Panda, and Kai-Chieh Yang. 2017. In-capture mobile video distortions: A study of subjective behavior and objective algorithms. *IEEE Transactions on Circuits and Systems for Video Technology* 28, 9 (2017), 2061–2077.

[12] Video Quality Experts Group et al. 2000. Final report from the video quality experts group on the validation of objective models of video quality assessment. In *VQEG meeting, Ottawa, Canada, March, 2000*.

[13] Kaiming He, Xiangyu Zhang, Shaoqing Ren, and Jian Sun. 2016. Deep residual learning for image recognition. In *Proceedings of the IEEE/CVF Conference on Computer Vision and Pattern Recognition*. 770–778.

[14] Vlad Hosu, Franz Hahn, Mohsen Jenadeleh, Hanhe Lin, Hui Men, Tamás Szirányi, Shujun Li, and Dietmar Saupe. 2017. The Konstanz natural video database (KoNViD-1k). In *IEEE International Conference on Quality of Multimedia Experience (QoMEX)*. 1–6.

[15] Vlad Hosu, Hanhe Lin, Tamas Sziranyi, and Dietmar Saupe. 2020. KonIQ-10k: An ecologically valid database for deep learning of blind image quality assessment. *IEEE Transactions on Image Processing* 29 (2020), 4041–4056.

[16] Xun Huang and Serge Belongie. 2017. Arbitrary style transfer in real-time with adaptive instance normalization. In *Proceedings of the IEEE/CVF International Conference on Computer Vision*. 1501–1510.

[17] Hassan Ismail Fawaz, Benjamin Lucas, Germain Forestier, Charlotte Pelletier, Daniel F Schmidt, Jonathan Weber, Geoffrey I Webb, Lhassane Idoumghar, Pierre-Alain Muller, and François Petitjean. 2020. Inceptiontime: Finding alexnet for time series classification. *Data Mining and Knowledge Discovery* 34, 6 (2020), 1936–1962.

[18] Woojae Kim, Jongyoo Kim, Sewoong Ahn, Jinwoo Kim, and Sanghoon Lee. 2018. Deep video quality assessor: From spatio-temporal visual sensitivity to a convolutional neural aggregation network. In *Proceedings of the European Conference on Computer Vision*. 219–234.

[19] Jari Korhonen. 2019. Two-level approach for no-reference consumer video quality assessment. *IEEE Transactions on Image Processing* 28, 12 (2019), 5923–5938.

[20] Jari Korhonen, Yicheng Su, and Junyong You. 2020. Blind natural video quality prediction via statistical temporal features and deep spatial features. In *Proceedings of the 28th ACM International Conference on Multimedia*. 3311–3319.

[21] Tengchuan Kou, Xiaohong Liu, Wei Sun, Jun Jia, Xiongkuo Min, Guangtao Zhai, and Ning Liu. 2023. Stablevqa: A deep no-reference quality assessment model for video stability. In *Proceedings of the 31st ACM International Conference on Multimedia*. 1066–1076.

[22] Bowen Li, Weixia Zhang, Meng Tian, Guangtao Zhai, and Xianpei Wang. 2022. Blindly assess quality of in-the-wild videos via quality-aware pre-training and motion perception. *IEEE Transactions on Circuits and Systems for Video Technology* 32, 9 (2022), 5944–5958.

[23] Dingquan Li, Tingting Jiang, and Ming Jiang. 2019. Quality assessment of in-the-wild videos. In *Proceedings of the 27th ACM International Conference on Multimedia*. 2351–2359.

[24] Dingquan Li, Tingting Jiang, and Ming Jiang. 2021. Unified quality assessment of in-the-wild videos with mixed datasets training. *International Journal of Computer Vision* 129 (2021), 1238–1257.

[25] Xuelong Li, Qun Guo, and Xiaoqiang Lu. 2016. Spatiotemporal statistics for video quality assessment. *IEEE Transactions on Image Processing* 25, 7 (2016), 3329–3342.

[26] Zutong Li and Lei Yang. 2022. DCVQE: A Hierarchical Transformer for Video Quality Assessment. In *Proceedings of the Asian Conference on Computer Vision*. 2562–2579.

[27] Weisi Lin and C-C Jay Kuo. 2011. Perceptual visual quality metrics: A survey. *Journal of Visual Communication and Image Representation* 22, 4 (2011), 297–312.

[28] Zhuang Liu, Hanzi Mao, Chao-Yuan Wu, Christoph Feichtenhofer, Trevor Darrell, and Saining Xie. 2022. A convnet for the 2020s. In *Proceedings of the IEEE/CVF Conference on Computer Vision and Pattern Recognition*. 11976–11986.

[29] Ze Liu, Jia Ning, Yue Cao, Yixuan Wei, Zheng Zhang, Stephen Lin, and Han Hu. 2022. Video swin transformer. In *Proceedings of the IEEE/CVF Conference on Computer Vision and Pattern Recognition*. 3202–3211.

[30] Zhuoqi Ma, Nannan Wang, Xinbo Gao, and Jie Li. 2018. From reality to perception: genre-based neural image style transfer.. In *International Joint Conference on Artificial Intelligence*. 3491–3497.

[31] Pavan C Madhusudana, Neil Birkbeck, Yilin Wang, Balu Adsumilli, and Alan C Bovik. 2023. Conviqt: Contrastive video quality estimator. *IEEE Transactions on Image Processing* (2023).

[32] Anish Mittal, Michele A Saad, and Alan C Bovik. 2015. A completely blind video integrity oracle. *IEEE Transactions on Image Processing* 25, 1 (2015), 289–300.

[33] Mikko Nuutinen, Toni Virtanen, Mikko Vaahteranoksa, Tero Vuori, Pirkko Oittinen, and Jukka Häkkinen. 2016. CVD2014—A database for evaluating no-reference video quality assessment algorithms. *IEEE Transactions on Image Processing* 25, 7 (2016), 3073–3086.

[34] Adam Paszke, Sam Gross, Francisco Massa, Adam Lerer, James Bradbury, Gregory Chanan, Trevor Killeen, Zeming Lin, Natalia Gimelshein, Luca Antiga, et al. 2019. Pytorch: An imperative style, high-performance deep learning library. *Advances in Neural Information Processing Systems* 32 (2019).

[35] Michele A Saad, Alan C Bovik, and Christophe Charrier. 2014. Blind prediction of natural video quality. *IEEE Transactions on image Processing* 23, 3 (2014), 1352–1365.

[36] Kalpana Seshadrinathan and Alan C Bovik. 2011. Temporal hysteresis model of time varying subjective video quality. In *IEEE International Conference on Acoustics, Speech and Signal Processing*. 1153–1156.

[37] Zeina Sinno and Alan Conrad Bovik. 2018. Large-scale study of perceptual video quality. *IEEE Transactions on Image Processing* 28, 2 (2018), 612–627.

[38] Wei Sun, Xiongkuo Min, Wei Lu, and Guangtao Zhai. 2022. A deep learning based no-reference quality assessment model for ugc videos. In *Proceedings of the 30th ACM International Conference on Multimedia*. 856–865.

[39] Ahmed Telili, Sid Ahmed Fezza, Wassim Hamidouche, and Hanene FZ Brachemi Meftah. 2023. 2BiVQA: Double bi-lstm-based video quality assessment of ugc videos. *ACM Transactions on Multimedia Computing, Communications and Applications* 20, 4 (2023), 1–22.

[40] Zhengzhong Tu, Yilin Wang, Neil Birkbeck, Balu Adsumilli, and Alan C Bovik. 2021. UGC-VQA: Benchmarking blind video quality assessment for user generated content. *IEEE Transactions on Image Processing* 30 (2021), 4449–4464.

[41] Zhengzhong Tu, Xiangxu Yu, Yilin Wang, Neil Birkbeck, Balu Adsumilli, and Alan C Bovik. 2021. RAPIQUE: Rapid and accurate video quality prediction of user generated content. *IEEE Open Journal of Signal Processing* 2 (2021), 425–440.

[42] Ashish Vaswani, Noam Shazeer, Niki Parmar, Jakob Uszkoreit, Llion Jones, Aidan N Gomez, Łukasz Kaiser, and Illia Polosukhin. 2017. Attention is all you need. *Advances in Neural Information Processing Systems* 30 (2017).

[43] Yilin Wang, Junjie Ke, Hossein Talebi, Joong Gon Yim, Neil Birkbeck, Balu Adsumilli, Peyman Milanfar, and Feng Yang. 2021. Rich features for perceptual quality assessment of UGC videos. In *Proceedings of the IEEE/CVF Conference on Computer Vision and Pattern Recognition*. 13435–13444.

[44] Haoning Wu, Chaofeng Chen, Jingwen Hou, Liang Liao, Annan Wang, Wenxiu Sun, Qiong Yan, and Weisi Lin. 2022. Fast-vqa: Efficient end-to-end video quality assessment with fragment sampling. In *European Conference on Computer Vision*. 538–554.

[45] Haoning Wu, Chaofeng Chen, Liang Liao, Jingwen Hou, Wenxiu Sun, Qiong Yan, Jinwei Gu, and Weisi Lin. 2023. Neighbourhood representative sampling for efficient end-to-end video quality assessment. *IEEE Transactions on Pattern Analysis and Machine Intelligence* (2023).

[46] Haoning Wu, Chaofeng Chen, Liang Liao, Jingwen Hou, Wenxiu Sun, Qiong Yan, and Weisi Lin. 2023. Discovqa: temporal distortion-content transformers for video quality assessment. *IEEE Transactions on Circuits and Systems for Video Technology* (2023).

[47] Haoning Wu, Erli Zhang, Liang Liao, Chaofeng Chen, Jingwen Hou, Annan Wang, Wenxiu Sun, Qiong Yan, and Weisi Lin. 2023. Exploring video quality

assessment on user generated contents from aesthetic and technical perspectives. In *Proceedings of the IEEE/CVF International Conference on Computer Vision*. 1–8.

[48] Haoning Wu, Erli Zhang, Liang Liao, Chaofeng Chen, Jingwen Hou, Annan Wang, Wenxiu Sun, Qiong Yan, and Weisi Lin. 2023. Towards explainable in-the-wild video quality assessment: a database and a language-prompted approach. In *Proceedings of the 31st ACM International Conference on Multimedia*. 1045–1054.

[49] Jianjun Xiang, Mei Yu, Gangyi Jiang, Haiyong Xu, Yang Song, and Yo-Sung Ho. 2020. Pseudo video and refocused images-based blind light field image quality assessment. *IEEE Transactions on Circuits and Systems for Video Technology* 31, 7 (2020), 2575–2590.

[50] Sidi Yang, Tianhe Wu, Shuwei Shi, Shanshan Lao, Yuan Gong, Mingdeng Cao, Jiahao Wang, and Yujiu Yang. 2022. Maniqa: Multi-dimension attention network for no-reference image quality assessment. In *Proceedings of the IEEE/CVF Conference on Computer Vision and Pattern Recognition*. 1191–1200.

[51] Zhengyi Yang, Yuanjie Dang, Jianjun Xiang, and Peng Chen. 2023. STAN: Spatio-Temporal Alignment Network for No-Reference Video Quality Assessment. In *International Conference on Artificial Neural Networks*. 160–171.

[52] Zhenqiang Ying, Maniratnam Mandal, Deepti Ghadiyaram, and Alan Bovik. 2021. Patch-VQ:'Patching Up'the video quality problem. In *Proceedings of the IEEE/CVF Conference on Computer Vision and Pattern Recognition*. 14019–14029.

[53] Junyong You. 2021. Long short-term convolutional transformer for no-reference video quality assessment. In *Proceedings of the 29th ACM International Conference on Multimedia*. 2112–2120.

[54] Junyong You, Jari Korhonen, Andrew Perkis, and Touradj Ebrahimi. 2011. Balancing attended and global stimuli in perceived video quality assessment. *IEEE Transactions on Multimedia* 13, 6 (2011), 1269–1285.

[55] Kun Yuan, Zishang Kong, Chuanchuan Zheng, Ming Sun, and Xing Wen. 2023. Capturing co-existing distortions in user-generated content for no-reference video quality assessment. In *Proceedings of the 31st ACM International Conference on Multimedia*. 1098–1107.

[56] Ao-Xiang Zhang, Yuan-Gen Wang, Weixuan Tang, Leida Li, and Sam Kwong. 2023. A spatial–temporal video quality assessment method via comprehensive HVS simulation. *IEEE Transactions on Cybernetics* (2023).

[57] Weixia Zhang, Kede Ma, Guangtao Zhai, and Xiaokang Yang. 2021. Uncertainty-aware blind image quality assessment in the laboratory and wild. *IEEE Transactions on Image Processing* 30 (2021), 3474–3486.

[58] Zicheng Zhang, Wei Wu, Wei Sun, Danyang Tu, Wei Lu, Xiongkuo Min, Ying Chen, and Guangtao Zhai. 2023. MD-VQA: Multi-dimensional quality assessment for UGC live videos. In *Proceedings of the IEEE/CVF Conference on Computer Vision and Pattern Recognition*. 1746–1755.

[59] Kai Zhao, Kun Yuan, Ming Sun, and Xing Wen. 2023. Zoom-vqa: patches, frames and clips integration for video quality assessment. In *Proceedings of the IEEE/CVF Conference on Computer Vision and Pattern Recognition*. 1302–1310.